PCCP

Unconventional Gas-Phase Synthesis of Biphenyl and its Atropisomeric Methyl-Substituted Derivatives

Journal:	*Physical Chemistry Chemical Physics*
Manuscript ID	CP-ART-02-2024-000765.R2
Article Type:	Paper
Date Submitted by the Author:	03-Jun-2024
Complete List of Authors:	Goettl, Shane; University of Hawaii He, Chao; University of Hawaii Yang, Zhenghai; University of Hawaii Kaiser, Ralf; University of Hawaii Somani, Ankit; Ruhr-Universität Bochum Portela-Gonzalez, Adrian; Ruhr-Universität Bochum Sander, Wolfram; Ruhr-Universität Bochum Sun, Bing-Jian; National Dong Hwa University Fatimah, Siti; National Dong Hwa University Kadam, Komal; National Dong Hwa University Chang, Agnes; National Dong Hwa University

Data Availability Statement

The data that support the findings of this study are available in the article and the supplementary information. Additional data are available from the corresponding authors upon reasonable request.

Unconventional Gas-Phase Synthesis of Biphenyl and its Atropisomeric Methyl-Substituted Derivatives

Author List

Shane J. Goettl,[1] Chao He,[1] Zhenghai Yang,[1] Ralf I. Kaiser,[1]* Ankit Somani,[2] Adrian Portela-Gonzalez,[2] Wolfram Sander,[2]* Bing-Jian Sun,[3] Siti Fatimah,[3] Komal P. Kadam,[3] Agnes H. H. Chang[3]*

Affiliations

[1] *Department of Chemistry, University of Hawai'i at Mānoa, Honolulu, HI 96822, USA*

[2] *Lehrstuhl für Organische Chemie II, Ruhr-Universität Bochum, 44801 Bochum, Germany*

[3] *Department of Chemistry, National Dong Hwa University, Shoufeng, Hualien 974, Taiwan*

*Correspondance: ralfk@hawaii.edu, wolfram.sander@rub.de, hhchang@gms.ndhu.edu.tw

Abstract

The biphenyl molecule ($C_{12}H_{10}$) acts as a fundamental molecular backbone in the stereoselective synthesis of organic materials due to its inherent twist angle causing atropisomerism in substituted derivatives and in molecular mass growth processes in circumstellar environments and combustion systems. Here, we reveal an unconventional low-temperature phenylethynyl addition–cyclization–aromatization mechanism for the gas-phase preparation of biphenyl ($C_{12}H_{10}$) along with *ortho*-, *meta*-, and *para*-substituted methylbiphenyl ($C_{13}H_{12}$) derivatives through crossed molecular beams and computational studies providing compelling evidence on their formation via bimolecular gas-phase reactions of phenylethynyl radicals (C_6H_5CC, X^2A_1) with 1,3-butadiene-d_6 (C_4D_6), isoprene ($CH_2C(CH_3)CHCH_2$), and 1,3-pentadiene ($CH_2CHCHCHCH_3$). The dynamics involve de-facto barrierless phenylethynyl radical additions via submerged barriers followed by facile cyclization and hydrogen shift prior to hydrogen atom emission and aromatization to racemic mixtures (*ortho, meta*) of biphenyls in overall exoergic reactions. These findings not only challenge our current perception of biphenyls as high temperature markers in combustion systems and astrophysical environments, but also identify biphenyls as fundamental building blocks of complex polycyclic

aromatic hydrocarbons (PAHs) such as coronene ($C_{24}H_{12}$) eventually leading to carbonaceous nanoparticles (soot, grains) in combustion systems and in deep space thus affording critical insight into the low-temperature hydrocarbon chemistry in our universe.

Introduction

Following the discovery of its non-planarity in 1949[1], the biphenyl ($C_{12}H_{10}$) molecule—a hydrocarbon consisting of two benzene rings bridged by a carbon-carbon single bond—has garnered substantial attention from the organic synthetic, physical organic chemistry, materials science, and medicinal chemistry communities for its role as a vital molecular building block of natural products[2], chiroptical nanomaterials[3,4], enantioselective catalysts[5,6], and photoswitches[7] (Fig. 1). This significance stems from steric hindrance prohibiting free rotation around the bridging single bond between the phenyl moieties thus producing a dihedral angle of 44° and rotational barrier of 6 kJ mol^{-1} [8,9]. The stability of the twisted structure arises from a balance between the steric repulsion of opposing *ortho* hydrogens and the electrostatic interaction of the π-orbitals[10]. Substituting a single hydrogen of biphenyl induces axial chirality of the molecule and atropisomerism—two key traits for stereoselectivity[11,12]. *Ortho* substituents induce the greatest effect, as a replacement of a single hydrogen by a methyl moiety ($–CH_3$) increases the phenyl–phenyl dihedral angle by 25°, while methyl substitution in the *meta* position offers little to no change in the angle[13-15]. These properties afford a precise tunability of the biphenyl backbone thus providing unique characteristics and functions which make biaryls vital components of organo- and enantioselective catalysts used in, e.g., asymmetric counteranion-directed catalysis (ACDC) toward the synthesis of chiral drugs and assembly of enantiomerically pure ligands[5,16].

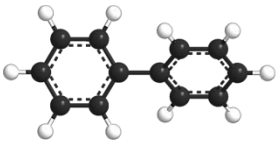
[1]

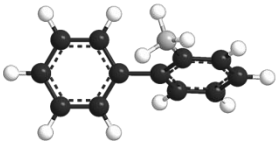
[2]

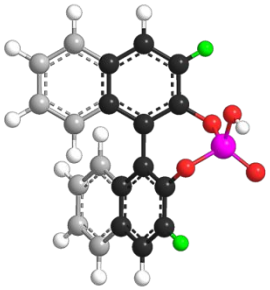
[3]

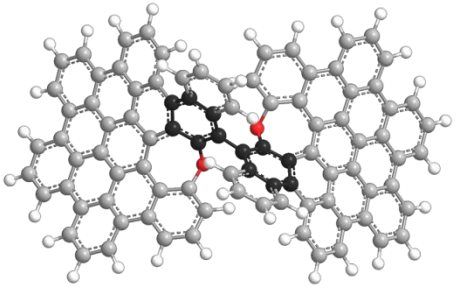
[4]

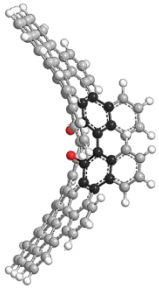

Fig. 1 Molecular structures of biphenyl **[1]** and 2-methylbiphenyl **[2**] as well as examples of a chiral phosphoric acid (CPA) catalyst **[3]** and a 1,1′-binaphthyl-2,2′-diol (BINOL) nanographene **[4]** emphasizing the twisted biphenyl backbone. Carbon atoms in the biphenyl moiety are colored as black, other carbons are gray, oxygen is red, phosphorus is magenta, hydrogen is white, and side groups are green.

The aromatic biphenyl molecule is also of fundamental interest to the astrochemistry and combustion science communities as a precursor to complex polycyclic aromatic hydrocarbons (PAHs) via the hydrogen abstraction – acetylene addition (HACA)[17] and phenyl addition – dehydrocyclization (PAC)[18] mechanisms forming, e.g., phenanthrene ($C_{14}H_{10}$) and triphenylene ($C_{18}H_{12}$), respectively, and eventually carbonaceous nanoparticles referred to as interstellar grains[19] and soot[20]. In deep space, PAHs have been suggested to account for up to 30 % of the cosmic carbon budget and are implicated as carriers of diffuse interstellar bands (DIBs)[21] and unidentified infrared (UIR) bands[22]. Sophisticated analyses of carbonaceous chondrites such as Allende[23] and Murchison[24] revealed the presence of PAHs, including biphenyl, presumably formed in circumstellar envelopes of carbon-rich asymptotic giant branch (AGB) stars along with planetary nebulae as their descendants[25]. The formation mechanisms in these high temperature environments are similar to those in hydrocarbon-rich combustion flames, where biphenyl has been observed in flames of alkanes, such as propane[26], *n*-butane[27], and *n*-dodecane[28], alkenes, e.g. ethylene[29,30], as well as aromatics like benzene[31-33], toluene[34], and styrene[35]. Traditionally, a bottom-up synthesis of biphenyl proceeds through the reaction of phenyl radicals (C_6H_5) with benzene (C_6H_6)[36] via an entrance barrier of 11 kJ mol^{-1} [37]. Consequently, the aforementioned gas-phase preparation of biphenyl is constrained to high temperature environments where entrance barriers can be overcome easily. While this results in biphenyl playing a vital role in combustion[38-43] and circumstellar[44-46] models for molecular mass growth processes of PAHs at elevated temperatures, pathways to biphenyl in low-temperature environments such as in hydrocarbon rich atmospheres of planets and their moons like Titan and in cold molecular clouds such as TMC-1 and OMC-1 have been discounted and hence remained elusive to date. These pathways are critical to prepare a population of aromatics in low-temperature environments to quantitatively replicate the observed PAH abundances in deep space[47-49].

Herein, we report on the gas-phase formation of biphenyl ($C_{12}H_{10}$) and its *ortho*-, *meta*-, and *para*-substituted methylbiphenyl ($C_{13}H_{12}$) derivatives via the bimolecular reactions of the phenylethynyl radical (C_6H_5CC, X^2A_1) with 1,3-butadiene-d_6 (C_4D_6), isoprene (2-methyl-1,3-butadiene, $CH_2C(CH_3)CHCH_2$), and 1,3-pentadiene (1-methyl-1,3-butadiene, $CH_2CHCHCHCH_3$)

under single collision conditions utilizing a crossed molecular beams machine coupled with high level *ab initio* electronic structure and statistical calculations (reactions (1)–(3)). Each elementary reaction proceeds de-facto without an entrance barrier through a van-der-Waals complex in the entrance channel with all transition states leading eventually to biphenyls residing lower in energy than the separated reactants; hence, these systems are rapidly accessible in low-temperature environments such as cold molecular clouds where temperatures as low as 10 K reside[50]. This pathway constitutes a unique, low-temperature framework for the formation of (substituted) biphenyls and PAHs as racemic building blocks in molecular mass growth processes to carbonaceous nanostructures, while challenging conventional wisdom of biphenyls as high temperature markers in combustion and circumstellar chemistry.

$$C_6H_5CC\ (101\ amu) + C_4D_6\ (60\ amu) \rightarrow C_{12}H_4D_6\ (160\ amu) + H\ (1\ amu) \quad (1a)$$

$$\rightarrow C_{12}H_5D_5\ (159\ amu) + D\ (2\ amu) \quad (1b)$$

$$C_6H_5CC\ (101\ amu) + CH_2C(CH_3)CHCH_2\ (68\ amu) \rightarrow C_{13}H_{12}\ (168\ amu) + H\ (1\ amu) \quad (2)$$

$$C_6H_5CC\ (101\ amu) + CH_2CHCHCHCH_3\ (68\ amu) \rightarrow C_{13}H_{12}\ (168\ amu) + H\ (1\ amu) \quad (3)$$

Methods

Experimental Methods

Reactions of phenylethynyl radicals (C_6H_5CC, X^2A_1) with 1,3-butadiene-d_6 (C_4D_6, 98.9 % D atom, CDN Isotopes), isoprene ($CH_2C(CH_3)CHCH_2$, 99 %, Sigma-Aldrich), and 1,3-pentadiene ($CH_2CHCHCHCH_3$, 96 %, TCI Chemicals) were conducted under single collision conditions using the crossed molecular beams technique.[51] Each reaction was done at two different collision energies by using either helium (He, 99.9999 %, Matheson) or neon (Ne, 99.9999 %, Matheson) as a seeding gas for the phenylethynyl beam. Briefly, a (2-bromoethynyl)benzene (C_6H_5CCBr) precursor was purified by multiple freeze–pump–thaw cycles and placed inside the primary source chamber where it was seeded at a fraction of 0.5 % in helium or neon at a backing pressure of 500 Torr. The ensuing gas mixture was fed through a Proch-Trickl pulsed valve[52] operating at −450 V and 120 Hz giving open times of 80 μs. The precursor was then photodissociated by 193 nm photons from an excimer laser (Coherent, COMPex 110) at 60 Hz and 10 mJ per pulse, creating a phenylethynyl radical beam which passed through a skimmer and was velocity selected by a chopper wheel resulting in a peak velocity (v_p) of 1765 ± 26 and 896 ± 10 m s^{-1} and a speed ratio (S) of 9.8 ± 1.1 and 14.0 ± 1.7 for the helium-seeded and neon-seeded reactions, respectively. The

phenylethynyl beam crossed perpendicularly with pulsed beams of 1,3-butadiene-d_6 (v_p = 750 ± 10 m s^{-1}, S = 8.0 ± 0.2), isoprene (v_p = 721 ± 20 m s^{-1}, S = 8.5 ± 0.6), and 1,3-pentadiene (v_p = 711 ± 20 m s^{-1}, S = 8.5 ± 0.7) at backing pressures of 550, 450, and 350 Torr, respectively, and pulsed valve parameters of −400 V, 120 Hz, and 80 μs open times. These reactions resulted in collision energies (E_C) of 68.9 ± 1.5, 72.7 ± 1.3, and 74.5 ± 1.5 kJ mol^{-1} and center-of-mass (CM) angles (Θ_{CM}) of 15.0 ± 0.4, 16.3 ± 0.5, and 15.8 ± 0.5°, respectively, for the helium-seeded reactions, while the neon-seeded cases gave E_C values of 25.8 ± 0.5, 26.8 ± 0.6, and 26.7 ± 0.7 kJ mol^{-1} and Θ_{CM} values of 27.1 ± 0.5, 29.2 ± 0.6, and 28.8 ± 0.9° (Table S1).

Reactive scattering products were collected by a triply differentially pumped mass spectrometric detector which is rotatable within the plane defined by both reactant beams. Neutral products were ionized at 80 eV and an emission current of 2 mA with a Brink-type[53] electron impact ionizer. The consequential ions were filtered by a quadrupole mass spectrometer (QMS, Extrel 150QC) in the time-of-flight (TOF) mode at a constant mass-to-charge ratio (m/z). Up to 1.8 × 10^6 TOF spectra were taken at each angle in 2.5° steps between 9 ≤ Θ ≤ 44° with respect to the phenylethynyl beam (Θ = 0°). Laboratory angular distributions for each system were created by integrating the TOF spectra and normalizing to the CM angles. To gain information on the reaction dynamics, a forward convolution routine creating user-defined CM translational energy ($P(E_T)$) and angular ($T(\theta)$) flux distributions was used to fit the laboratory angular distributions and TOF spectra in an iterative process.[54,55] These functions were used to develop a flux contour map, shown as $I(u, \theta) \sim P(u) \times T(\theta)$,[56] which portrays an overall image of the outcome of the reaction.

Computational Methods

The H loss channels of the reactions of phenylethynyl radicals (C_6H_5CC, X^2A_1) with 1,3-butadiene-d_6 (C_4D_6), isoprene ($CH_2C(CH_3)CHCH_2$), and 1,3-pentadiene ($CH_2CHCHCHCH_3$) on adiabatic doublet ground-state potential energy surfaces were explored, along with the phenylacetylene (C_6H_5CCD) formation path in the phenylethynyl–1,3-butadiene-d_6 system. The geometries of collision complexes, cyclized and hydrogen-shifted intermediates, transition states, and H loss products, were optimized with density functional wB97X-D[57]/cc-pVTZ calculations. Their coupled cluster CCSD(T)[58-60]/cc-pVTZ energies with wB97X-D/cc-pVTZ zero-point energy correction were then obtained. Single-point higher level (multi-configuration) energy has been

shown to yield good results for various closed and open-shell systems,[61-65] where the methods of CCSD(T)//B3LYP, G3//B3LYP, G3//B3LYP, and G3//*w*B97X-D, respectively, were employed. Intrinsic reaction coordinate (IRC) calculations have been carried out for the collision complexes **i1**, **i5**, **i9**, **i13**, and **i17**—the structures of which are discussed in the *Potential Energy Surfaces* section—back to reactants by density functional *w*B97X-D. GAUSSIAN16[66] programs were facilitated in the *ab initio* electronic structure calculations. The energy dependent RRKM (Rice−Ramsperger−Kassel−Marcus) rate constants[67] were computed for the likely atomic hydrogen loss products—including 4- 5- and 6-membered ring species—on doublet surfaces at various experimental collision energies and at 0.0 kJ mol^{-1}. The species involved were treated as a collection of harmonic oscillators. The saddle-point approach[67,68] was utilized to estimate the number of states of transition states, and density of states of collision complexes and intermediates with *w*B97X-D/cc-pVTZ harmonic frequencies and CCSD(T)/cc-pVTZ energies. In order to obtain branching ratios for all accessible products, complete reaction paths are required. Preliminary calculations illustrate, for instance, there are at least 16 paths for the collision complex **i5** (detailed in the *Potential Energy Surfaces* section) to isomerize, which means it is not practical to locate complete paths. However, it is feasible to estimate branching ratios among products by comparing the bottleneck (smallest) rate constant along **p1**, **p2**, and **p10** formation paths, which strongly indicates **p1** (biphenyl) is the major product. In order to get a quantitative result, the product branching ratios at zero collision energy were computed by solving the rate equations derived from *ab initio* reaction paths as in Figures S4, S5, and S6, respectively, with the Runge-Kutta method. The concentration evolution with time was thus obtained for every species involved, in which the asymptotic value of concentration is taken as branching ratio with collision complex initial concentration assumed to be 1.

Results & Discussion

Laboratory Frame

Reactive scattering time-of-flight (TOF) spectra (Fig. 2) were obtained at two different collision energies for the reactions of phenylethynyl (C_6H_5CC) radicals with 1,3-butadiene-d_6 (C_4D_6), isoprene ($CH_2C(CH_3)CHCH_2$), and 1,3-pentadiene ($CH_2CHCHCHCH_3$). First, signal was observed for the bimolecular reaction of phenylethynyl (C_6H_5CC) with 1,3-butadiene-d_6 (C_4D_6) at mass-to-charge ratios (m/z) of 160 ($C_{12}H_4D_6^+$, $^{13}CC_{11}H_5D_5^+$, $^{13}CC_{11}H_3D_6^+$), 159 ($C_{12}H_5D_5^+$,

$C_{12}H_3D_6^+$, $^{13}CC_{11}H_4D_5^+$, $^{13}CC_{11}H_2D_6^+$), and 158 ($C_{12}H_4D_5^+$, $C_{12}H_2D_6^+$, $^{13}CC_{11}H_5D_4^+$, $^{13}CC_{11}H_3D_5^+$, $^{13}CC_{11}HD_6^+$) for both high (E_C = 68.9 ± 1.5 kJ mol^{-1}) and low (E_C = 25.8 ± 0.5 kJ mol^{-1}) collision energies. In both cases, the TOFs at distinct m/z ratios overlap after scaling (Fig. S1) with m/z = 160 collected at a level of 13 ± 5 % compared to m/z = 159; thus, signal at m/z = 160 likely arises from ^{13}C-substituted $C_{12}H_5D_5^+$ accounting for natural isotopic abundance of about 1.1 % for ^{13}C, while that at m/z = 159 originates from $C_{12}H_5D_5^+$ coupled with atomic deuterium loss (reaction (1b)). This verifies that the hydrogen (deuterium) loss occurs solely from the 1,3-butadiene reactant. Since electron impact ionization at 80 eV was applied to ionize reactively scattered products, the counts observed at m/z = 158 result from dissociative electron impact ionization of the parent $C_{12}H_5D_5$ species in the ionizer. TOF spectra were then collected at m/z = 159 at center-of-mass (CM) angles (Θ_{CM}) of 14.3 ± 0.4 (Fig. 2d) and 26.3 ± 0.5° (Fig. 2j) with respect to the phenylethynyl beam for high and low collision energies, respectively. The high E_C TOFs are very narrow, spanning only about 150 μs, while the low E_C TOFs are much broader, spanning about 300 μs. TOFs were also acquired at higher and lower angles in 2.5° steps in order to create laboratory angular distributions (LAD, Figs. 2a and 2g), which are nearly symmetric about Θ_{CM}, indicating indirect reaction dynamics through $C_{12}H_5D_6$ intermediate(s). A strongly forward or backward peaking of the LAD with respect to Θ_{CM} would indicate rather direct scattering dynamics, which were not observed here.

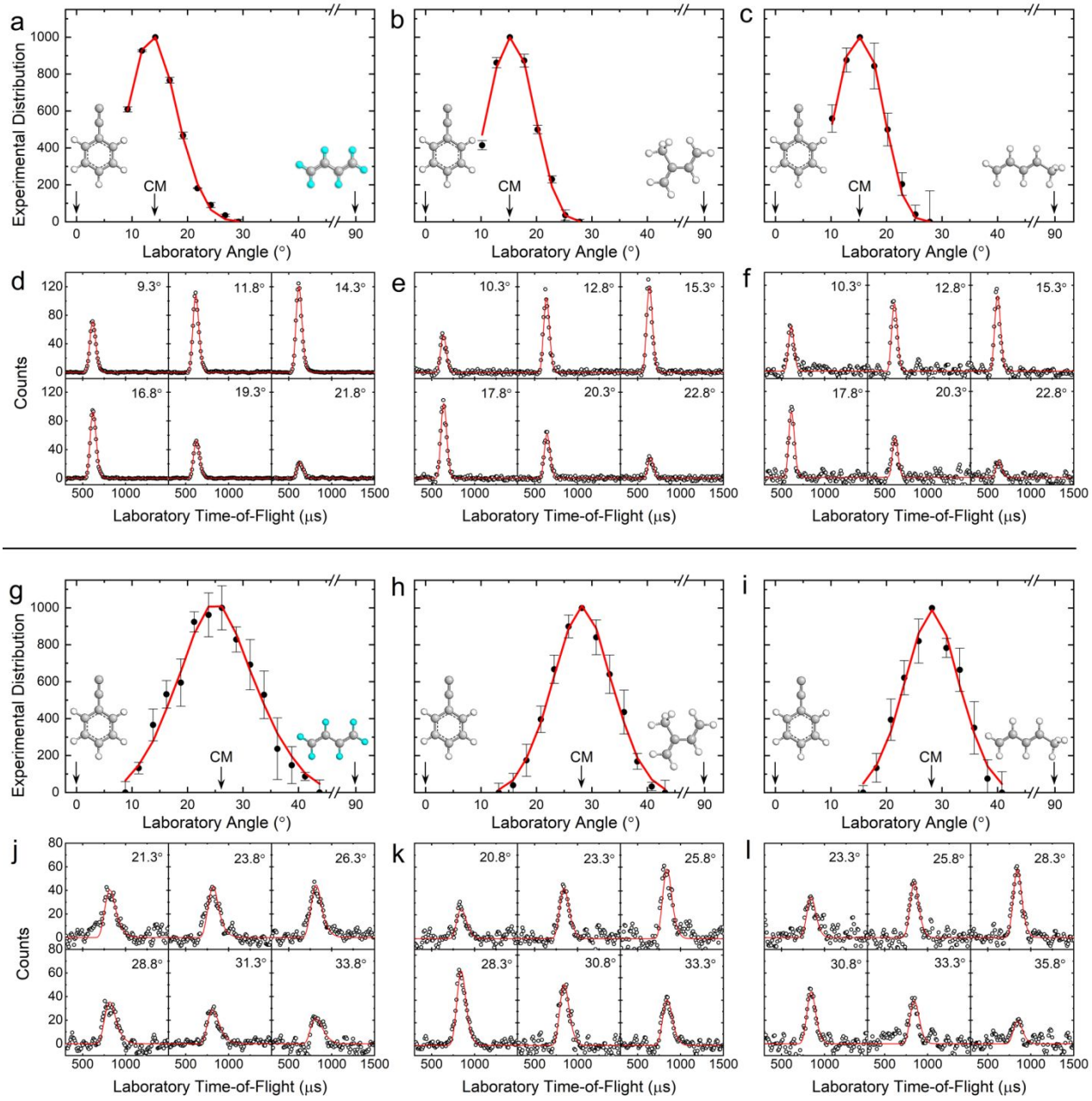

Fig. 2 Laboratory angular distributions (LADs) (**a–c, g–i**) and time-of-flight spectra (TOFs) (**d–f, j–l**) recorded at mass-to-charge (m/z) = 159, 168, and 168 for the reactions of phenylethynyl (C_6H_5CC) with 1,3-butadiene-d_6 (C_4D_6, **a, d, g, j**), isoprene ($CH_2C(CH_3)CHCH_2$, **b, e, h, k**), and 1,3-pentadiene ($CH_2CHCHCHCH_3$, **c, f, i, l**), respectively. CM represents the center-of-mass angle, and 0° and 90° define the directions of the phenylethynyl and 1,3-butadiene-d_6/isoprene/1,3-pentadiene beams, respectively. The black circles depict the data and red lines the fits. Reactions were done with high (**a–f**) and low (**g–l**) collision energies. Carbon atoms are colored gray, hydrogens are white, and deuterium atoms are light blue.

For both high (72.7 ± 1.3 kJ mol^{-1}) and low (26.8 ± 0.6 kJ mol^{-1}) collision energies in the reaction of phenylethynyl (C_6H_5CC) with isoprene ($CH_2C(CH_3)CHCH_2$), signal was observed at m/z = 169 ($^{13}CC_{12}H_{12}^+$), 168 ($C_{13}H_{12}^+$, $^{13}CC_{12}H_{11}^+$), and 167 ($C_{13}H_{11}^+$, $^{13}CC_{12}H_{10}^+$). These peaks overlap after scaling revealing that all three masses arise from a single channel (Fig. S2). Signal at m/z = 169 shows a level of 12 ± 5 % compared to m/z = 168 which is indicative of natural ^{13}C-substituted $C_{13}H_{12}^+$ species, while the peak at m/z = 168 originates from ionized $C_{13}H_{12}$ along with atomic hydrogen (reaction (2)). The counts observed at m/z = 167 result from dissociative electron impact ionization of the parent $C_{13}H_{12}$ species in the ionizer. Signal for the reaction of phenylethynyl with the 1,3-pentadiene ($CH_2CHCHCHCH_3$) isomer at E_C = 74.5 ± 1.5 and 26.7 ± 0.9 kJ mol^{-1} was much lower (Fig. S3) with signal only detected at m/z = 168 and 167 (reaction (3)). Background intensity from the (2-bromoethynyl)benzene precursor at m/z = 154 prevented detection of reactive scatting signal for the possible methyl loss channel. For both the isoprene and 1,3-pentadiene systems, TOFs were collected at m/z = 168 at CM angles of 15.3 ± 0.5 (Fig. 2e) and 15.3 ± 0.5° (Fig. 2f) for high E_C and 28.3 ± 0.6 (Fig. 2k) and 28.3 ± 0.9° (Fig. 2l) for low E_C, respectively. Much like the 1,3-butadiene-d_6 system, the TOFs for the C_5H_8 isomer reactions at high collision energies are very narrow at about 150 μs wide, while those at low collision energies are about twice the width. The LADs are also quite similar, with forward–backward symmetry about Θ_{CM} implying indirect reaction dynamics leading to $C_{13}H_{12}$ product(s) along with atomic hydrogen through $C_{13}H_{13}$ intermediate(s) (Figs. 2b–c and 2h–i).

Center-of-Mass Frame

With the identification of the $C_{12}H_5D_5$ product(s) coupled with deuterium loss from the phenylethynyl–1,3-butadiene-d_6 system, as well as $C_{13}H_{12}$ product(s) via hydrogen loss from the phenylethynyl–isoprene/1,3-pentadiene reactions, we now attempt an identification of the nature of the intermediates and products along with the overall reaction mechanisms. This is achieved by converting the laboratory data (TOF spectra, LAD) to the CM reference frame[69], producing the CM product translational energy ($P(E_T)$) and angular ($T(\theta)$) flux distributions (Fig. 3) and merging these data with electronic structure calculations (Figs. 4–6). For all three reactions and collision energies, the laboratory data could be fit with a single channel corresponding to product masses of 159 amu ($C_{12}H_5D_5$) plus 2 amu (D) (phenylethynyl–1,3-butadiene-d_6) and 168 amu ($C_{13}H_{12}$) plus 1 amu (H) (phenylethynyl–isoprene/1,3-pentadiene).

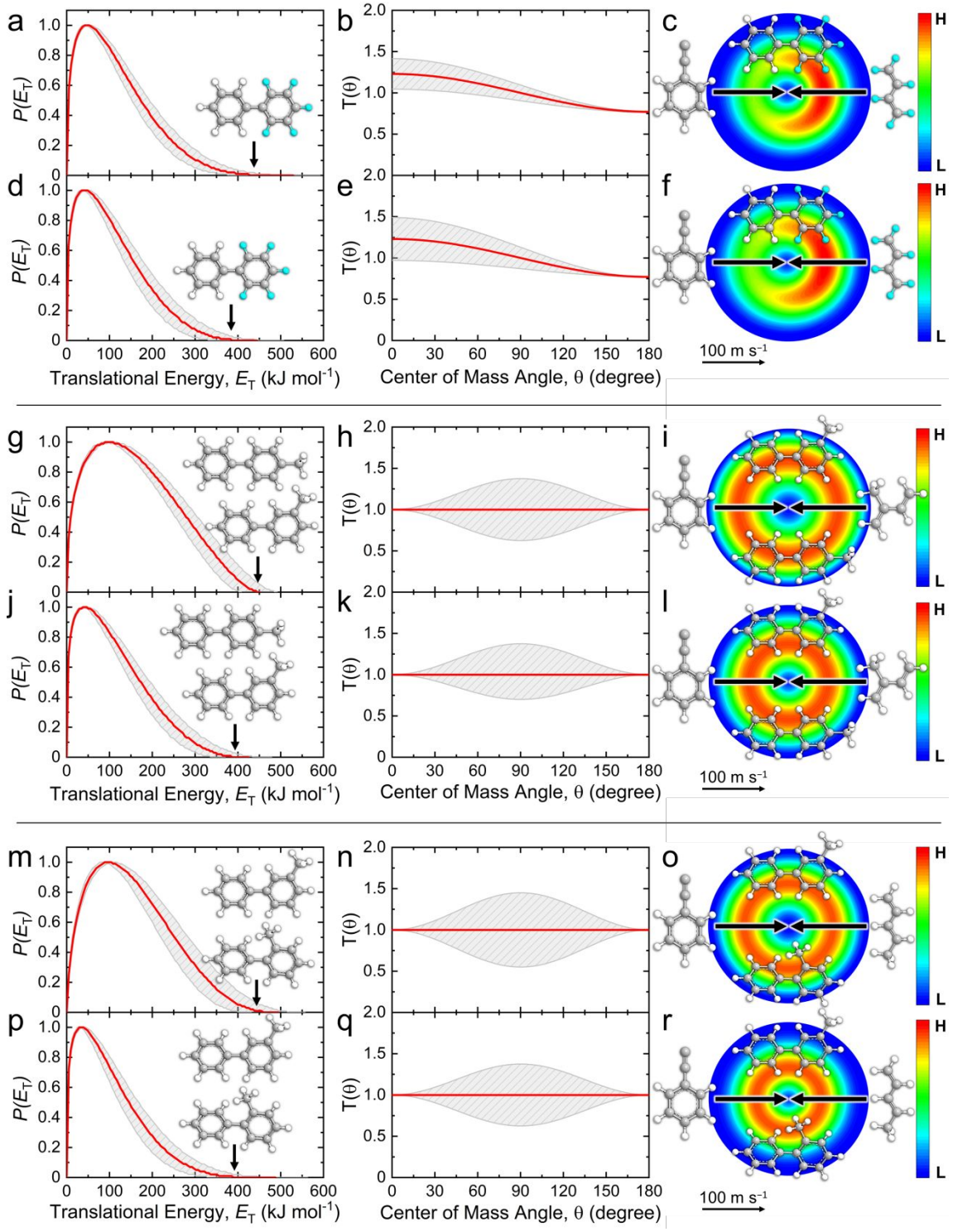

Fig. 3 CM product translational energy (**a, d, g, j, m, p**) and angular (**b, e, h, k, n, q**) flux distributions, as well as the associated flux contour maps (**c, f, i, l, o, r**) leading to the formation of $C_{12}H_5D_5$, $C_{12}H_{13}$, and $C_{12}H_{13}$ isomers in the reactions of phenylethynyl (C_6H_5CC) with 1,3-butadiene-d_6 (C_4D_6, **a–f**), isoprene ($CH_2C(CH_3)CHCH_2$, **g–l**), and 1,3-pentadiene ($CH_2CHCHCHCH_3$, **m–r**). Red lines define the best-fit functions while shaded areas provide the error limits. The flux contour map represents the intensity of the reactively scattered products as a function of product velocity (u) and scattering angle (θ), and the color bar indicates flux gradient from high (H) to low (L) intensity. Carbon atoms are colored gray, hydrogens are white, and deuterium atoms are light blue.

In case of reaction (1), the $P(E_T)$ extends up to 423 ± 50 and 382 ± 54 kJ mol^{-1} for high and low collision energies, respectively (Figs. 3a and 3d). Utilizing energy conservation for those products born without internal excitation, given by $\Delta_r G = E_C - E_{max}$, the reaction energy ($\Delta_r G$) can be obtained by subtracting the maximum translational energy (E_{max}) from the collision energy (E_C) providing similar values of −354 ± 52 and −356 ± 55 kJ mol^{-1} at high and low collision energies. The $P(E_T)$ depicts a maximum at about 45 kJ mol^{-1} at both collision energies suggesting that $C_{12}H_5D_5$ product(s) are formed via a tight exit transition state involving substantial electron density rearrangement from the decomposing complex to the final products[70]. The angular flux distributions show intensity over the full angular range, reinforcing the implication of indirect scattering dynamics through $C_{12}H_5D_5$ intermediate(s) (Fig. 3b and 3e). The $T(\theta)$ also display a slight forward asymmetry with an intensity ratio $I(0°)/I(180°)$ of about (1.6 ± 0.3):1.0, which suggests the existence of at least one channel where complex formation takes place but the lifetime is too short to allow multiple rotations[71]. These findings for both collision energies are reflected in the flux contour maps (Figs. 3c and 3f).

For reaction (2), the $P(E_T)$ provides E_{max} values of 441 ± 41 and 382 ± 49 kJ mol^{-1} yielding reaction energies of −368 ± 42 and −355 ± 50 kJ mol^{-1} for high and low E_C, respectively, while the $P(E_T)$ for reaction (3) affords reaction energies of −380 ± 60 and −358 ± 61 kJ mol^{-1} (Figs. 3g, 3j, 3m, and 3p). At high collision energy, the $P(E_T)$ for both reaction (2) and reaction (3) peak at about 95 kJ mol^{-1} while the $P(E_T)$ peaks at about 35 kJ mol^{-1} at low collision energy; therefore, both reactions (2) and (3) involve a tight exit transition state leading to $C_{13}H_{12}$ product(s) coupled with atomic hydrogen loss. Inspecting the angular flux distributions (Figs. 3h, 3k, 3n, and 3q), the $T(\theta)$ for reactions (2) and (3) feature isotropic scattering in which there is equal intensity at all angles. This reveals the formation of long-lived $C_{13}H_{13}$ intermediate(s) with lifetime(s) longer than their rotational period(s). These results are mirrored in the flux contour maps (Figs. 3i, 3l, 3o, and 3r). Overall, the reactions to form $C_{13}H_{12}$ are strongly exoergic by 355 ± 50 to 380 ± 60 kJ mol^{-1}.

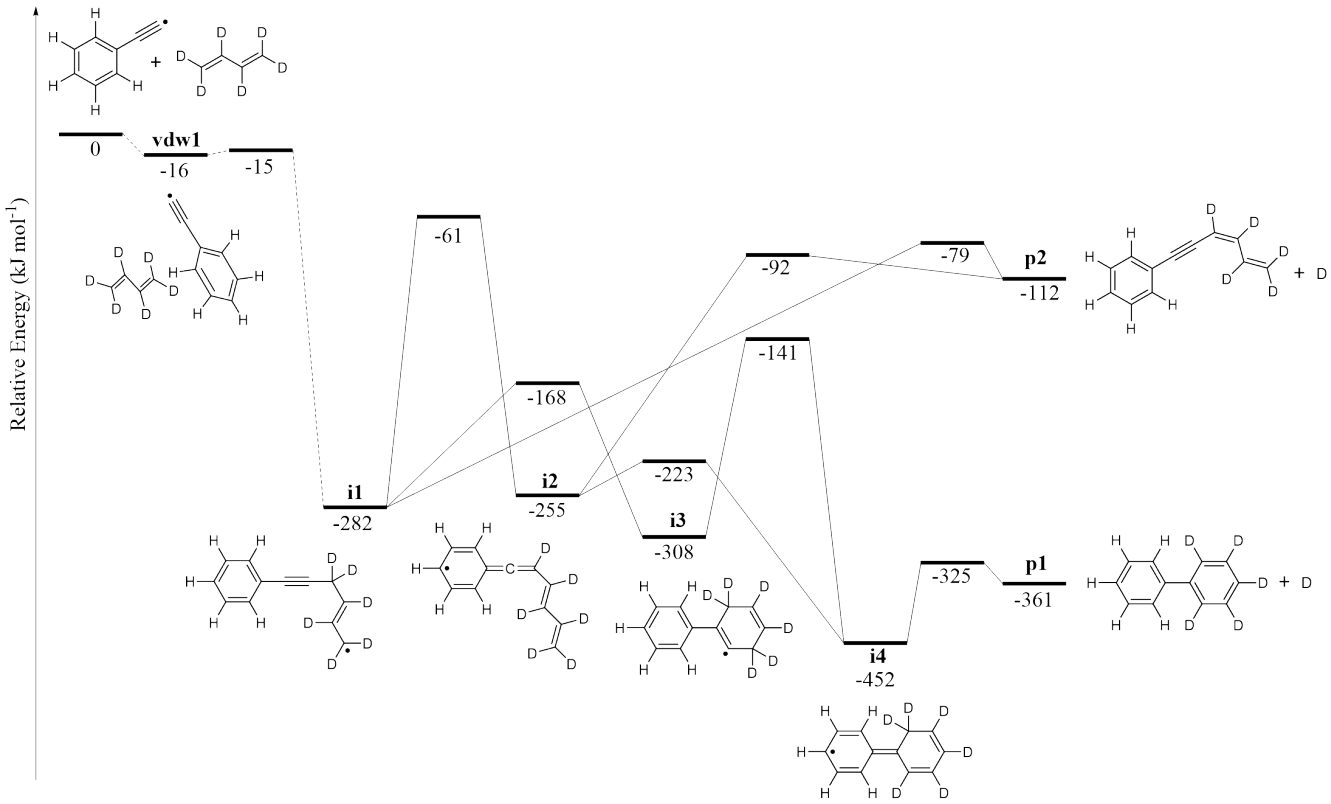

Fig. 4 Schematic potential energy surface for the reaction of phenylethynyl (C_6H_5CC) with 1,3-butadiene-d_6 (C_4D_6) obtained with CCSD(T)/cc-pVTZ//wB97XD/cc-pVTZ calculations.

Potential Energy Surfaces

The nature of the products and reaction pathways are now elucidated by combining our experimental results with electronic structure and statistical calculations. These potential energy surfaces (PES) were computed for the intermediates, reactants, and transition states of each system (Figs. 4–6 and S4–S6). Rate constants were calculated exploiting Rice–Ramsperger–Kassel–Marcus (RRKM) theory[72] at the experimental collision energies, as well as at 0 kJ mol^{-1} to account for interstellar conditions (Tables S2–S4). The differences in energetics between deuterated and non-deuterated species are minor.

For reaction (1b), the experiment provides a reaction energy (−354 ± 52; −356 ± 55 kJ mol^{-1}) which coincides with the calculated energy of biphenyl-d_5 ($C_{12}H_5D_5$, **p1**) plus atomic deuterium (−361 kJ mol^{-1}, Fig. 4). The initial step of reaction starts with the formation of a van-der-Waals complex (**vdw1**) in the entrance channel. The latter isomerizes via phenylethynyl radical addition to one of the double bonds of 1,3-butadiene-d_6 leading to methylallyl radical collision complex **i1**, which is stabilized by 282 kJ mol^{-1} with respect to the separated reactants.

The barrier to addition of only 1 kJ mol^{-1} is well below the energy of the separated reactants (submerged barrier).

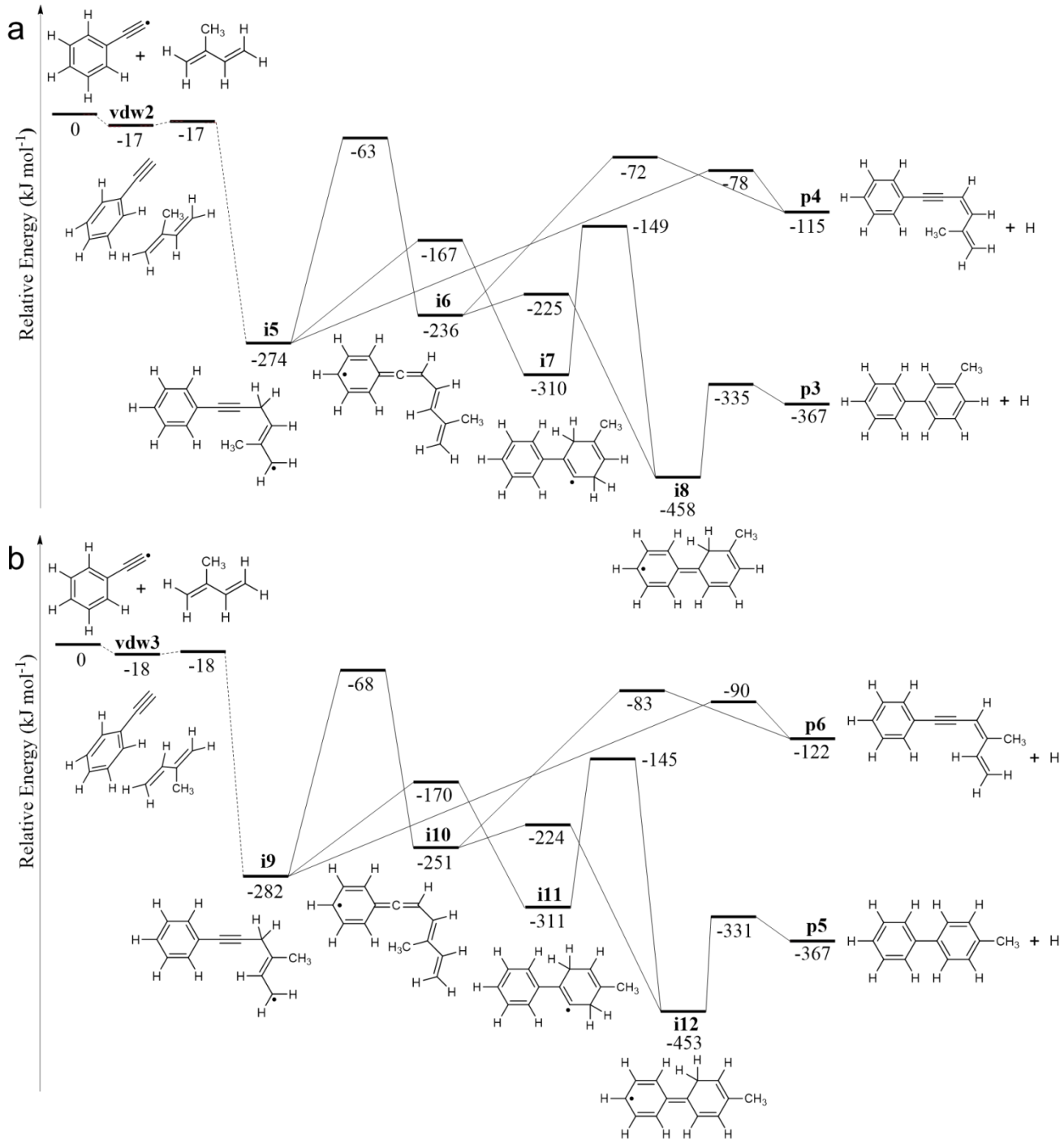

Fig. 5 Schematic potential energy surface for the reaction of phenylethynyl (C_6H_5CC) with isoprene ($CH_2C(CH_3)CHCH_2$) obtained with CCSD(T)/cc-pVTZ//wB97XD/cc-pVTZ calculations for phenylethynyl addition to the C4 (**a**) and C1 (**b**) carbons of isoprene.

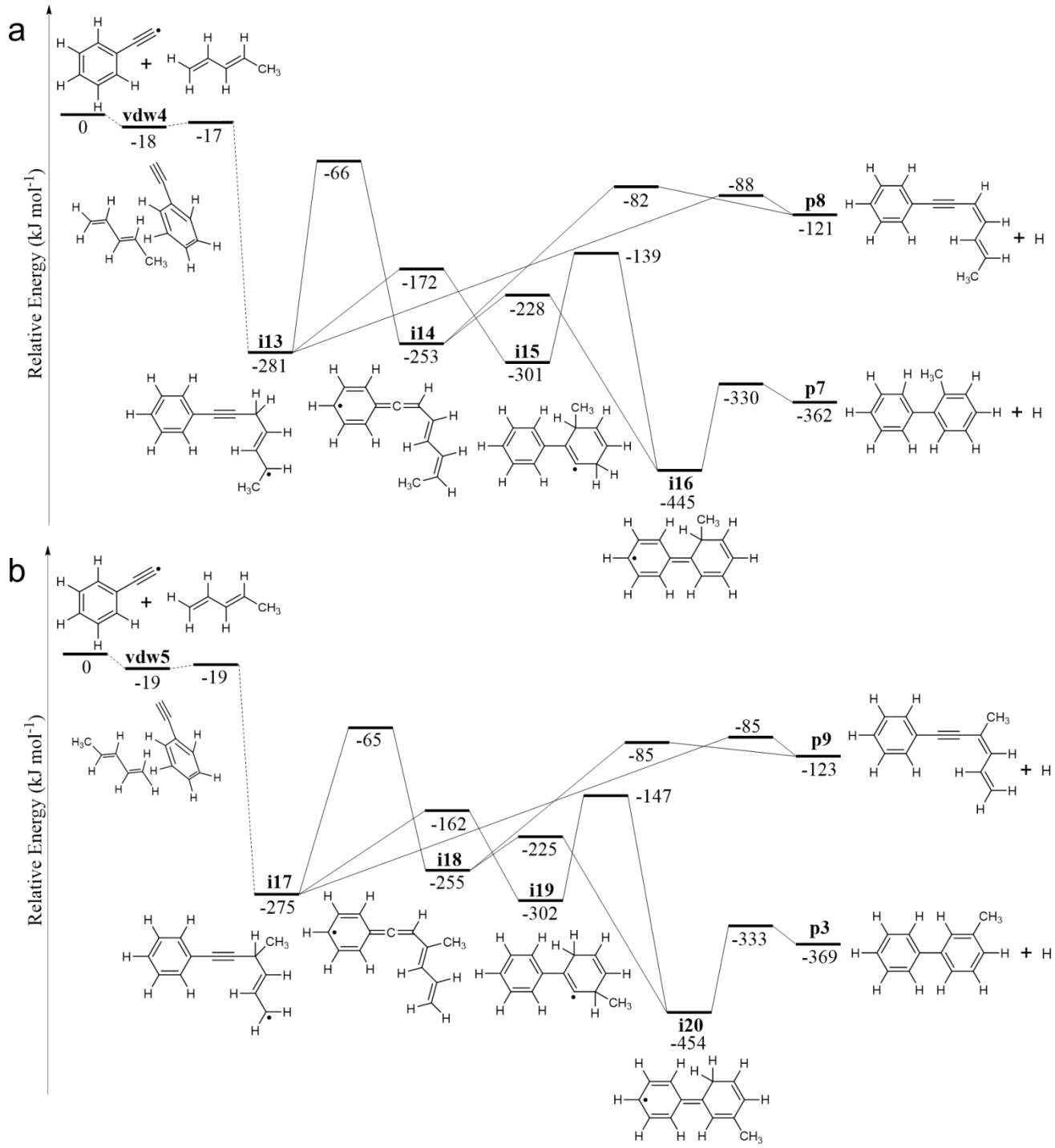

Fig. 6 Schematic potential energy surface for the reaction of phenylethynyl (C_6H_5CC) with 1,3-pentadiene ($CH_2CHCHCHCH_3$) obtained with CCSD(T)/cc-pVTZ//wB97XD/cc-pVTZ calculations for phenylethynyl addition to the C1 (**a**) and C4 (**b**) carbons of 1,3-pentadiene.

While there are two possible pathways leading to **p1**, the energetically favorable route involves six-membered ring closure of the radical side chain (**i1** → **i3**), [1,2] deuterium shift on the newly formed cyclic group (**i3** → **i4**), and finally deuterium loss (**i4** → **p1**) over a tight exit barrier. While the experimental reaction energy matches that of **p1**, it is possible that 3,5-hexadien-1-yn-1-ylbenzene (**p2**) is veiled within the lower energy portion of the $P(E_T)$ and acts as a secondary product. There are also two pathways leading to **p2**, with the most likely being a simple addition–elimination mechanism featuring deuterium loss from methylallyl-type radical **i1**. The rate constants reinforce these conclusions, where the six-membered ring closure via the methylallyl-type radical **i1** → phenylcyclohexadienyl radical **i3** pathway (k_1), subsequent [1,2] deuterium shift, and atomic deuterium loss is at least three orders of magnitude faster than the alternative reaction routes (k_2, k_3) from the methylallyl-type radical **i1** as discussed above, while routes involving the formation of a 5-membered ring are also slower (Table S2, Fig. S4). Overall, these results provide compelling evidence on the formation of at least biphenyl-d_5 via the reaction of the phenylethynyl radical with 1,3-butadiene-d_6.

Reactions (2) and (3) follow a similar pattern as for reaction (1b), with the methyl group on the isoprene and 1,3-pentadiene reactants acting as a spectator, i.e. the methyl moiety is not actively participating in the chemical dynamics of the reactions. By changing the position of the methyl group on the 1,3-butadiene backbone from the C1 to the C2 carbon atom, the resulting methyl position on the biphenyl moiety can be tuned. For reaction (2) (Fig. 5), the phenylethynyl radical can add to either of the terminal double-bonded carbons on the isoprene backbone. The initially formed van-der-Waals complexes (**vdW2, vdW3**) may isomerize. The phenylethynyl radical addition to the C4 (Fig. 5a) or C1 (Fig. 5b) carbon of isoprene leads eventually to 3-methylbiphenyl ($C_{13}H_{12}$, **p3**) or 4-methylbiphenyl ($C_{13}H_{12}$, **p5**), respectively, plus atomic hydrogen through the most favorable pathways **i5** → **i7** → **i8** → **p3** or **i9** → **i11** → **i12** → **p5**, which are the methyl-substituted equivalents of the phenylethynyl–1,3-butadiene-d_6 route. The calculated reaction energies for **p3** (−367 kJ mol^{-1}) and **p5** (−367 kJ mol^{-1}) match nicely with the observed experimental reaction energies (−368 ± 42; −355 ± 50 kJ mol^{-1}). Likewise, for reaction (3), van-der-Waals complexes (**vdW4, vdW5**) can be accessed in the entrance channel, and their fate is dictated by an addition of the phenylethynyl radical via a submerged barrier to the doubly-bonded C1 (Fig. 6a) or C4 (Fig. 6b) carbon of 1,3-pentadiene leading eventually to 2-methylbiphenyl ($C_{13}H_{12}$, **p7**) or 3-methylbiphenyl ($C_{13}H_{12}$, **p3**), respectively, via hydrogen loss through the

phenylethynyl–isoprene equivalent **i13** → **i15** → **i16** → **p7** and **i17** → **i19** → **i20** → **p3** routes. The rate constants from the initial methylallyl-type radical collision complexes (**i5**/**i9**/**i13**/**i17**) also support this reasoning, with the cyclization step followed by [1,2] hydrogen shift and hydrogen atom loss giving rate constant values of up to eight orders of magnitude higher than alternate pathways (Tables S3–S4). Additionally, in all three reactions, the critical transition state in the formation of the monocyclic products is 53–73 kJ mol^{-1} higher in energy than for the biphenyl derivatives, indicating that the products **p2**, **p4**, **p6**, **p8**, and **p9** encompass only a minor fraction of reactive scattering signal, if any, which further reinforces the generation of biphenyl and its methyl-substituted derivatives as major products in the reactions of phenylethynyl radicals with 1,3-butadiene-d_6, isoprene, and 1,3-pentadiene (Fig. 7).

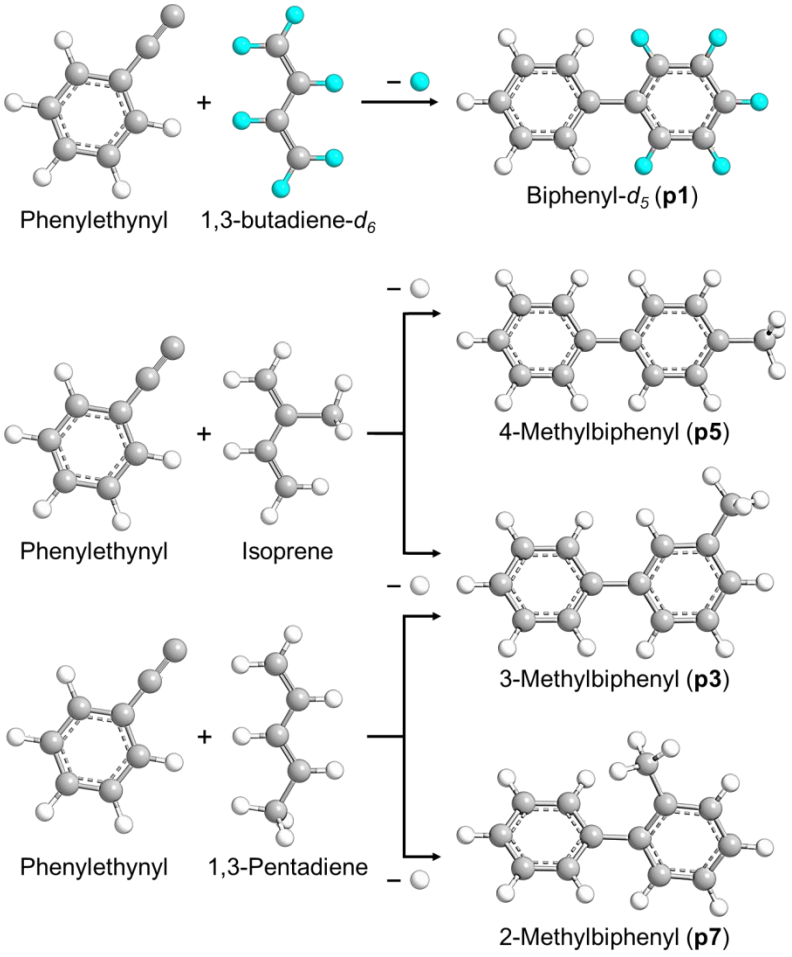

Fig. 7 Product channels for the reactions of phenylethynyl radicals (C_6H_5CC) with 1,3-butadiene-d_6 (C_4D_6), isoprene ($CH_2C(CH_3)CHCH_2$), and 1,3-pentadiene ($CH_2CHCHCHCH_3$). Carbon atoms are colored gray, hydrogens are white, and deuteriums are light blue.

Conclusion & Outlook

Overall, our combined crossed molecular beams and computational study on the bimolecular gas-phase reactions of phenylethynyl radicals (C_6H_5CC) with three molecules containing a 1,3-butadiene backbone—1,3-butadiene-d_6 (C_4D_6), isoprene ($CH_2C(CH_3)CHCH_2$), and 1,3-pentadiene ($CH_2CHCHCHCH_3$)—uncovered the unconventional formation of biphenyl and its *ortho*-, *meta*-, and *para*-substituted methylbiphenyl derivatives under single collision conditions. The reaction routes involve formation of van-der-Waals complexes in the entrance channels of the reactions followed by isomerization through addition of the phenylethynyl radical center via submerged barriers to the π-electron system of the secondary reactant at the terminal carbon atom(s) followed by facile ring closure and hydrogen shift isomerization prior to unimolecular decomposition of the reaction intermediates via atomic hydrogen loss. These patterns classify this reaction sequence as a low-temperature framework for the formation of (un)substituted biphenyls and PAHs as building blocks in molecular mass growth processes to carbonaceous nanostructures. Prototypes of successive reactions, of which the fundamental mechanisms have previously been explored[73-78], are featured in Fig. 8 eventually leading to the formation of coronene ($C_{24}H_{12}$)—a fundamental molecular building block in two-dimensional carbonaceous nanostructures—via hydrogen abstraction – acetylene addition (HACA), hydrogen abstraction – vinylacetylene addition (HAVA), and radical–radical reactions (RRR).

Essentially, this phenylethynyl addition–cyclization–aromatization mechanism serves as a versatile framework for tuning the position of an alkyl group within the biphenyl backbone to adjust chirality and dihedral angle for stereoselectivity. Further, the de-facto barrierless nature of reaction defies conventional wisdom that biphenyl symbolizes a high temperature marker in combustion and circumstellar chemistry as a product of, e.g., phenyl radicals with benzene[36]. This opens up (un)substituted biphenyl formation through previously overlooked reaction pathways in low-temperature environments such as cold molecular clouds and hydrocarbon-rich atmospheres of planets or their moons. While PAHs like biphenyl itself are difficult to explicitly detect in extraterrestrial environments due to the lack of a permanent dipole moment, *ortho*-, *meta*-, and/or *para*-substituted cyanobiphenyls acquire a significant dipole because of their cyano substituents. Hence, substituted biphenyls represent unique targets for unraveling the complex evolution of the cosmic carbon balance in low-temperature interstellar environments thus bringing us closer to an understanding of the aromatic universe we live in.

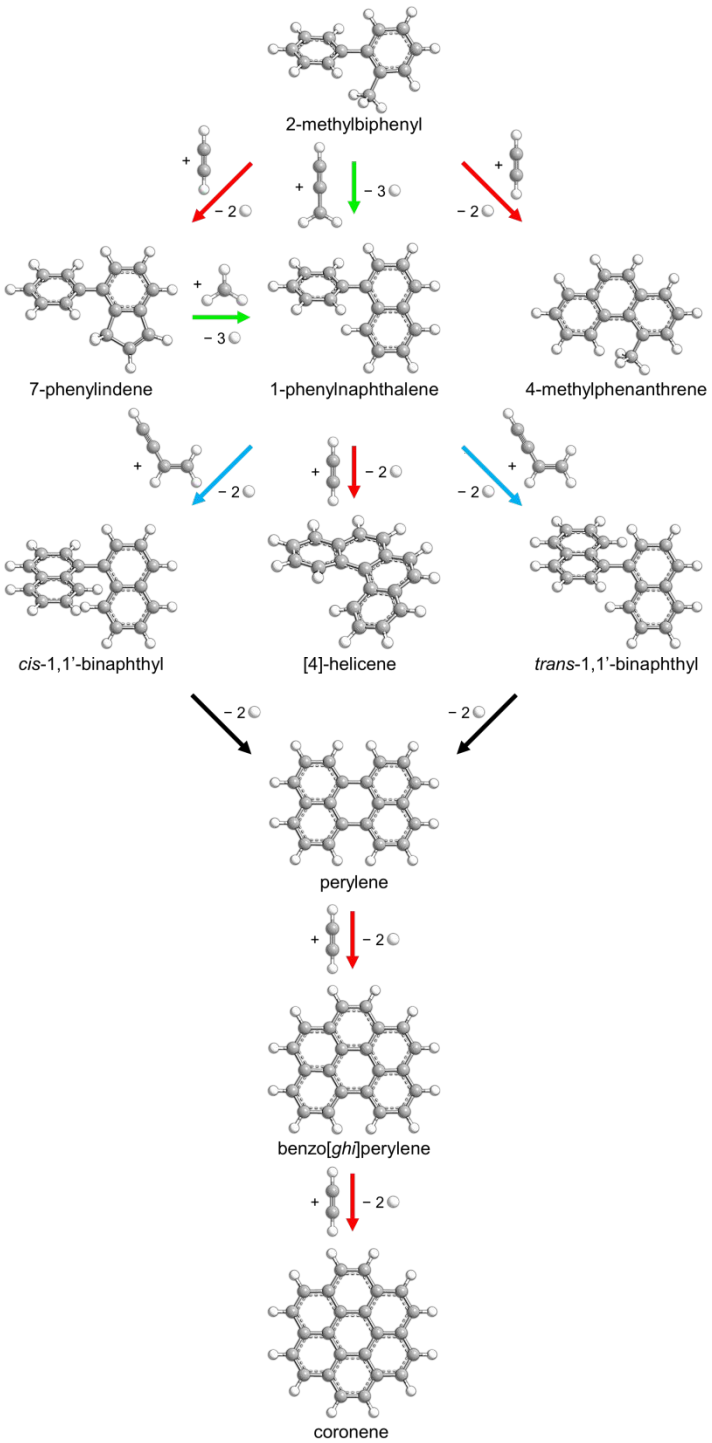

Fig. 8 Key role of methyl substituted biphenyls exploiting 2-methylbiphenyl as a prototype through the hydrogen abstraction – acetylene addition (HACA, red), hydrogen abstraction – vinylacetylene addition (HAVA, blue), and radical–radical reaction (RRR, green) mechanisms to the products 7-phenylindene, 4-methylphenanthrene, 1-phenylnaphthalene, and [4]-helicene, as well as the *cis*- and *trans*-1,1'-binaphthyl backbones of compounds **[3]** and **[4]** from Fig. 1 eventually leading to coronene—a molecular building block of two-dimensional nanostructures. Carbon atoms are colored gray and hydrogens are white.

Data Availability Statement

The data that support the findings of this study are available in the article and the supplementary information. Additional data are available from the corresponding authors upon reasonable request.

Author Contributions

R.I.K. designed and supervised the experiment; S.J.G., C.H., Z.Y., and A.S. performed the experimental measurements; A.P.-G. synthesized the experimental precursor; W.S. supervised the precursor synthesis; S.J.G. performed the data analysis; B.-J.S., S.F., and K.P.K. carried out the threoretical analysis; A.H.H.C. supervised the theoretical analysis; S.J.G., R.I.K., W.S., and A.H.H.C. wrote the paper.

Conflict of Interest

The authors declare no competing financial interest.

Acknowledgments

The experimental studies at the University of Hawaii were supported by the US Department of Energy, Basic Energy Sciences DE-FG02-03ER15411. The chemical synthesis at Ruhr-Universität Bochum was supported by the Deutsche Forschungsgemeinschaft (DFG, German Research Foundation) under Germany's Excellence Strategy-EXC-2033 390677874 RESOLV. BJS, SF, KPK. and AHHC thank the National Center for High-Performance Computing in Taiwan for providing the computer resources.

References

1 O. Bastiansen, *Acta Chem. Scand.*, 1949, **3**, 408-414.
2 T. Qin, S. L. Skraba-Joiner, Z. G. Khalil, R. P. Johnson, R. J. Capon and J. A. Porco, *Nat. Chem.*, 2015, **7**, 234-240.
3 S. Li, R. Li, Y.-K. Zhang, S. Wang, B. Ma, B. Zhang and P. An, *Chem. Sci.*, 2023, **14**, 3286-3292.
4 T. M. Fukunaga, T. Kato, K. Ikemoto and H. Isobe, *Proc. Natl. Acad. Sci. U. S. A.*, 2022, **119**, e2120160119.
5 L. C. Mayer, S. Heitsch and O. Trapp, *Acc. Chem. Res.*, 2022, **55**, 3345-3361.

6 T. A. Schmidt, S. Schumann, A. Ostertag and C. Sparr, *Angew. Chem., Int. Ed.*, 2023, DOI: https://doi.org/10.1002/anie.202302084, e202302084.

7 A. H. G. David, R. Casares, J. M. Cuerva, A. G. Campaña and V. Blanco, *J. Am. Chem. Soc.*, 2019, **141**, 18064-18074.

8 A. Almenningen, O. Bastiansen, L. Fernholt, B. N. Cyvin, S. J. Cyvin and S. Samdal, *J. Mol. Struct.*, 1985, **128**, 59-76.

9 O. Bastiansen and S. Samdal, *J. Mol. Struct.*, 1985, **128**, 115-125.

10 K. C. Park, L. R. Dodd, K. Levon and T. K. Kwei, *Macromolecules*, 1996, **29**, 7149-7154.

11 G. Bringmann, A. J. Price Mortimer, P. A. Keller, M. J. Gresser, J. Garner and M. Breuning, *Angew. Chem., Int. Ed.*, 2005, **44**, 5384-5427.

12 C. B. Roos, C.-H. Chiang, L. A. M. Murray, D. Yang, L. Schulert and A. R. H. Narayan, *Chem. Rev.*, 2023, **123**, 10641-10727.

13 J. P. Maier and D. W. Turner, *Faraday Discuss. Chem. Soc.*, 1972, **54**, 149-167.

14 J. J. Dynes, F. L. Baudais and R. K. Boyd, *Can. J. Chem.*, 1985, **63**, 1292-1299.

15 L. Andrews, R. T. Arlinghaus and C. K. Payne, *J. Chem. Soc., Faraday Trans. 2*, 1983, **79**, 885-895.

16 M. Mahlau and B. List, *Angew. Chem., Int. Ed.*, 2013, **52**, 518-533.

17 T. Yang, T. P. Troy, B. Xu, O. Kostko, M. Ahmed, A. M. Mebel and R. I. Kaiser, *Angew. Chem., Int. Ed.*, 2016, **55**, 14983-14987.

18 L. Zhao, M. B. Prendergast, R. I. Kaiser, B. Xu, U. Ablikim, M. Ahmed, B. J. Sun, Y. L. Chen, A. H. H. Chang and R. K. Mohamed, *Angew. Chem., Int. Ed.*, 2019, **131**, 17603-17611.

19 B. T. Draine, *Annu. Rev. Astron. Astrophys.*, 2003, **41**, 241-289.

20 J. W. Martin, M. Salamanca and M. Kraft, *Prog. Energy Combust. Sci.*, 2022, **88**, 100956.

21 W. W. Duley, *Faraday Discuss.*, 2006, **133**, 415-425.

22 A. M. Ricks, G. E. Douberly and M. A. Duncan, *Astrophys. J.*, 2009, **702**, 301.

23 L. Becker and T. E. Bunch, *Meteorit. Planet. Sci.*, 1997, **32**, 479-487.

24 T. N. Tingle, C. H. Becker and R. Malhotra, *Meteoritics*, 1991, **26**, 117-127.

25 F. L. Plows, J. E. Elsila, R. N. Zare and P. R. Buseck, *Geochim. Cosmochim. Acta*, 2003, **67**, 1429-1436.

26 N. M. Marinov, M. J. Castaldi, C. F. Melius and W. Tsang, *Combust. Sci. Technol.*, 1997, **128**, 295-342.

27 N. M. Marinov, W. J. Pitz, C. K. Westbrook, A. M. Vincitore, M. J. Castaldi, S. M. Senkan and C. F. Melius, *Combust. Flame*, 1998, **114**, 192-213.

28 T. Mitra, T. Zhang, A. D. Sediako and M. J. Thomson, *Combust. Flame*, 2019, **202**, 33-42.

29 R. P. Lindstedt and B. B. O. Waldheim, *Proc. Combust. Inst.*, 2013, **34**, 1861-1868.

30 A. Liu, C. E. Garcia, F. Sewerin, B. A. O. Williams and S. Rigopoulos, *Combust. Flame*, 2020, **221**, 384-400.

31 H. Richter, T. G. Benish, O. A. Mazyar, W. H. Green and J. B. Howard, *Proc. Combust. Inst.*, 2000, **28**, 2609-2618.

32 L. Zhao, W. Sun, J. Yang and B. Yang, *Combust. Flame*, 2018, **197**, 355-368.

33 A. Hamadi, W. Sun, S. Abid, N. Chaumeix and A. Comandini, *Combust. Flame*, 2022, **237**, 111858.

34 V. Detilleux and J. Vandooren, *J. Phys. Chem. A*, 2009, **113**, 10913-10922.

35 W. Yuan, Y. Li, P. Dagaut, J. Yang and F. Qi, *Combust. Flame*, 2015, **162**, 1868-1883.

36 F. Zhang, X. Gu and R. I. Kaiser, *J. Chem. Phys.*, 2008, **128**.

37 J. Park, S. Burova, A. S. Rodgers and M. C. Lin, *J. Phys. Chem. A*, 1999, **103**, 9036-9041.

38 J. Guo, P. Liu, E. Quadarella, K. Yalamanchi, I. Alsheikh, C. Chu, F. Liu, S. M. Sarathy, W. L. Roberts and H. G. Im, *Combust. Flame*, 2022, **246**, 112420.

39 A. Liu, Z. Gao, S. Rigopoulos, K. H. Luo and L. Zhu, *Fuel*, 2022, **317**, 122897.

40 T. Kathrotia, P. Oßwald, C. Naumann, S. Richter and M. Köhler, *Fuel*, 2021, **302**, 120736.

41 X. Shi, Q. Wang and A. Violi, *Combust. Flame*, 2020, **212**, 216-233.
42 T. Zhang and M. J. Thomson, *Combust. Flame*, 2018, **190**, 416-431.
43 J.-L. Consalvi, F. Liu, M. Kashif and G. Legros, *Combust. Flame*, 2017, **180**, 167-174.
44 D. K. Bohme, *Chem. Rev.*, 1992, **92**, 1487-1508.
45 I. Cherchneff, in *Molecules in Astrophysics: Probes and Processes*, ed. E. F. v. Dishoeck, Cambridge University Press, 1997, vol. 178, pp. 469-476.
46 P. Cau, *Astron. Astrophys.*, 2002, **392**, 203-213.
47 A. G. G. M. Tielens, *Annu. Rev. Astron. Astrophys.*, 2008, **46**, 289-337.
48 L. J. Allamandola, D. M. Hudgins and S. A. Sandford, *Astrophys. J.*, 1999, **511**, L115.
49 L. Zhao, R. I. Kaiser, B. Xu, U. Ablikim, M. Ahmed, M. M. Evseev, E. K. Bashkirov, V. N. Azyazov and A. M. Mebel, *Nat. Astron.*, 2018, **2**, 973-979.
50 S. T. Megeath, E. Allgaier, E. Young, T. Allen, J. L. Pipher and T. L. Wilson, *Astron. J.*, 2009, **137**, 4072.
51 X. Gu, Y. Guo and R. I. Kaiser, *Int. J. Mass Spectrom.*, 2005, **246**, 29-34.
52 D. Proch and T. Trickl, *Rev. Sci. Instrum.*, 1989, **60**, 713-716.
53 G. O. Brink, *Rev. Sci. Instrum.*, 1966, **37**, 857-860.
54 M. F. Vernon, Ph.D. Dissertation, University of California at Berkeley, 1983.
55 P. S. Weiss, Ph.D. Dissertation, University of California at Berkeley, 1985.
56 R. I. Kaiser, *Chem. Rev.*, 2002, **102**, 1309-1358.
57 J.-D. Chai and M. Head-Gordon, *Phys. Chem. Chem. Phys.*, 2008, **10**, 6615-6620.
58 G. D. Purvis, III and R. J. Bartlett, *J. Chem. Phys.*, 1982, **76**, 1910-1918.
59 C. Hampel, K. A. Peterson and H.-J. Werner, *Chem. Phys. Lett.*, 1992, **190**, 1-12.
60 P. J. Knowles, C. Hampel and H. J. Werner, *J. Chem. Phys.*, 1993, **99**, 5219-5227.
61 J. M. Simmie and K. P. Somers, *J. Phys. Chem. A*, 2015, **119**, 7235-7246.
62 B. M. Jones, F. Zhang, R. I. Kaiser, A. Jamal, A. M. Mebel, M. A. Cordiner and S. B. Charnley, *Proc. Natl. Acad. Sci. U. S. A.*, 2011, **108**, 452-457.
63 K. L. K. Lee, B. A. McGuire and M. C. McCarthy, *Phys. Chem. Chem. Phys.*, 2019, **21**, 2946-2956.
64 M. C. McCarthy, K. L. K. Lee, R. A. Loomis, A. M. Burkhardt, C. N. Shingledecker, S. B. Charnley, M. A. Cordiner, E. Herbst, S. Kalenskii, E. R. Willis, C. Xue, A. J. Remijan and B. A. McGuire, *Nat. Astron.*, 2021, **5**, 176-180.
65 S. J. Goettl, Z. Yang, S. Kollotzek, D. Paul, R. I. Kaiser, A. Somani, A. Portela-Gonzalez, W. Sander, A. A. Nikolayev, V. N. Azyazov and A. M. Mebel, *J. Phys. Chem. A*, 2023, **127**, 5723-5733.
66 M. J. Frisch, G. W. Trucks, H. B. Schlegel, G. E. Scuseria, M. A. Robb, J. R. Cheeseman, G. Scalmani, V. Barone, G. A. Petersson, H. Nakatsuji, X. Li, M. Caricato, A. V. Marenich, J. Bloino, B. G. Janesko, R. Gomperts, B. Mennucci, H. P. Hratchian, J. V. Ortiz, A. F. Izmaylov, J. L. Sonnenberg, Williams, F. Ding, F. Lipparini, F. Egidi, J. Goings, B. Peng, A. Petrone, T. Henderson, D. Ranasinghe, V. G. Zakrzewski, J. Gao, N. Rega, G. Zheng, W. Liang, M. Hada, M. Ehara, K. Toyota, R. Fukuda, J. Hasegawa, M. Ishida, T. Nakajima, Y. Honda, O. Kitao, H. Nakai, T. Vreven, K. Throssell, J. A. Montgomery Jr., J. E. Peralta, F. Ogliaro, M. J. Bearpark, J. J. Heyd, E. N. Brothers, K. N. Kudin, V. N. Staroverov, T. A. Keith, R. Kobayashi, J. Normand, K. Raghavachari, A. P. Rendell, J. C. Burant, S. S. Iyengar, J. Tomasi, M. Cossi, J. M. Millam, M. Klene, C. Adamo, R. Cammi, J. W. Ochterski, R. L. Martin, K. Morokuma, O. Farkas, J. B. Foresman and D. J. Fox, *Gaussian 16*, Revision B.01; Gaussian, Inc.: Wallingford, CT, 2016; see http://www.gaussian.com.
67 A. H. H. Chang, A. M. Mebel, X.-M. Yang, S. H. Lin and Y. T. Lee, *J. Chem. Phys.*, 1998, **109**, 2748-2761.
68 H. Eyring, S. H. Lin and S. M. Lin, *Basic Chemical Kinetics*, John Wiley & Sons, Inc., New York, 1980.
69 R. I. Kaiser, C. Ochsenfeld, D. Stranges, M. Head-Gordon and Y. T. Lee, *Faraday Discuss.*, 1998, **109**, 183-204.

70 J. Laskin and C. Lifshitz, *Journal of Mass Spectrometry*, 2001, **36**, 459-478.
71 W. B. Miller, S. A. Safron and D. R. Herschbach, *Discuss. Faraday Soc.*, 1967, **44**, 108-122.
72 R. A. Marcus, *J. Chem. Phys.*, 1952, **20**, 359-364.
73 D. S. N. Parker, R. I. Kaiser, O. Kostko and M. Ahmed, *ChemPhysChem*, 2015, **16**, 2091-2093.
74 C. He, R. I. Kaiser, W. Lu, M. Ahmed, V. S. Krasnoukhov, P. S. Pivovarov, M. V. Zagidullin, V. N. Azyazov, A. N. Morozov and A. M. Mebel, *Chem. Sci.*, 2023, **14**, 5369-5378.
75 T. Yang, R. I. Kaiser, T. P. Troy, B. Xu, O. Kostko, M. Ahmed, A. M. Mebel, M. V. Zagidullin and V. N. Azyazov, *Angew. Chem., Int. Ed.*, 2017, **129**, 4586-4590.
76 L. Zhao, R. Kaiser, W. Lu, B. Xu, M. Ahmed, A. N. Morozov, A. M. Mebel, A. H. Howlader and S. F. Wnuk, *Nat. Commun.*, 2019, **10**, 1-7.
77 L. Zhao, R. I. Kaiser, B. Xu, U. Ablikim, M. Ahmed, M. V. Zagidullin, V. N. Azyazov, A. H. Howlader, S. F. Wnuk and A. M. Mebel, *J. Phys. Chem. Lett.*, 2018, **9**, 2620-2626.
78 S. J. Goettl, L. B. Tuli, A. M. Turner, Y. Reyes, A. H. Howlader, S. F. Wnuk, P. Hemberger, A. M. Mebel and R. I. Kaiser, *J. Am. Chem. Soc.*, 2023, **145**, 15443-15455.